Full communication

Plastic derived carbon nanotubes for electrocatalytic oxygen reduction reaction: Effects of plastic feedstock and synthesis temperature

James Guo Sheng Moo[a,*], Andrei Veksha[a], Wen-Da Oh[b], Apostolos Giannis[a,c], W.D. Chanaka Udayanga[a,d], Sheng-Xuan Lin[a], Liya Ge[a], Grzegorz Lisak[a,d,**]

[a] Residues and Resource Reclamation Centre (R3C), Nanyang Environment and Water Research Institute (NEWRI), Nanyang Technological University, 1 Cleantech Loop, CleanTech One, Singapore 637141, Singapore
[b] School of Chemical Sciences, Universiti Sains Malaysia, 11800 Penang, Malaysia
[c] School of Environmental Engineering, Technical University of Crete, University Campus, 73100 Chania, Greece
[d] School of Civil and Environmental Engineering, Nanyang Technological University, 50 Nanyang Avenue, 639798, Singapore

ARTICLE INFO

ABSTRACT

Closing the resource loop by transforming plastic waste into higher value products is an important step for changing from a linear to circular economy. Using a sequential pyrolysis and catalytic chemical vapour deposition process, plastics have been successfully converted into carbon nanotubes (CNTs). Pure low density polyethylene (LDPE), polypropylene (PP) and mixed plastics (MP) were used as raw materials in the two-stage process. In the first stage, the plastics were pyrolysed at 600 °C. In the second stage, the non-condensable gases were converted into multi-walled CNTs over a Ni-based catalyst at two different temperatures, 500 and 800 °C. The influence of plastic feedstock and synthesis temperature on the performance of plastic-derived CNTs as electrode materials in electrocatalysis was investigated. The CNTs were evaluated as electrode materials for their heterogeneous electron transfer rate using a redox probe, which showed improved electrochemical behaviour. For oxygen reduction reaction (ORR), CNTs produced at 500 °C demonstrated superior performance compared to those produced at 800 °C. Influence of feedstock on electrocatalytic ORR activity of the as synthesised CNTs was marginal. Temperature was the governing factor influencing the properties of CNTs due to annealing and oxidation of edge defects generated during synthesis at higher temperatures.

1. Introduction

Recycling of plastic waste is one of the greatest challenges in municipal solid waste management domain [1,2] because they are typically present as a mixture of polymers [3–5]. Single-source and mixed plastics were converted via pyrolysis into simple molecules with subsequent recovery of value-added products [6] such as liquid fuels [7], precursors for organic synthesis of polymers [8] or carbon-based nanomaterials [9]. To synthesise carbon-based nanomaterials from plastics, several routes were proposed. In catalytic plastic pyrolysis, a catalyst can be added to plastics and the mixture is pyrolysed to produce solid carbon nanomaterials [10]. Alternatively, plastics are first decomposed in a pyrolysis reactor and afterwards carbon nanomaterials are synthesised in a separate reactor with a catalyst either before or after condensation of liquid pyrolysis products [11,12]. Pyrolysis followed by catalytic chemical vapour deposition have demonstrated the feasibility to reduce the volumetric mass of plastics and turn them into carbon-based nanomaterials [9,11–19], which can be utilized as fillers for polymer composites [14–16] or electrodes [18,19]. While some research has been conducted on the synthesis of CNTs from plastics, the application of such materials is barely studied. For instance, plastic waste-derived CNTs have been mainly restricted to applications in enhancing mechanical performance of polymer composites [14–16], rather than their intrinsic electrochemical properties as conductive carbons [18,19].

Electrocatalysts are needed as materials for manufacturing of electrodes [20,21]. Carbon based nanomaterials have been postulated to play an integral role as core electrode materials [21]. Owing to the large surface area and high number of active sites, carbon nanomaterials have been forecasted to participate in a range of electrochemical reactions [22,23]. This is particularly applicable to carbon nanotubes (CNTs), due to high conductivity, large number of active edge-sites and

---

high mechanical strength [24]. Since the discovery of CNTs, this carbon allotrope has found widespread applications in electronic materials [25]. Optimisation of the synthesis CNTs are often needed, due to the presence of carbonaceous fragments [26] and metallic impurities [27]. Specifically, CNTs have been used as fuel cell electrode materials for oxygen reduction reaction (ORR) [28,29], where operations are often conducted at extreme conditions.

In this work, mixed plastics are decomposed via pyrolysis and the non-condensable pyrolysis gases are converted into functional multi-walled CNTs via chemical vapour deposition using nickel-based catalyst. The waste-derived CNTs are tested as electrocatalysts in ORR. To date, few studies have related the conditions for synthesis of CNTs to the electrochemical performance [18,19]. The novelty of this study is the relation of the synthesis process to applications of the CNTs as electrodes for ORR. The effects of plastic feedstock (low density polyethylene (LDPE), polypropylene (PP) and mixed plastics (MP)) and synthesis temperature are examined on CNTs synthesis. The intrinsic (surface chemistry) and extrinsic (morphology and elemental content) properties are investigated to reveal the electrochemical properties as electrocatalyst for ORR.

2. Experimental

2.1. Synthesis of carbon nanotubes (CNTs)

Low density polyethylene (LDPE) from PTT Global Chemical Public Co. Ltd. (Thailand), polypropylene (PP) from Sinopec (China), polystyrene (PS) from Formosa Plastics Corp. (Taiwan) and polyethylene terephthalate (PET) from CR Chemicals Holdings Co. Ltd. (China) were used as raw materials. Chemical formulas of the polymers have been included in Scheme S1 in the Supplementary information. The following three carbon sources were used as precursors for CNTs synthesis: (1) LDPE (100%), (2) PP (100%) and (3) mixed plastics (MP). The mixed plastics contained LDPE (40%), PP (40%), PS (10%) and PET (10%). Nickel is a common catalyst for the synthesis of carbon nano-materials using chemical vapour deposition process [17,30]. The catalyst for CNTs synthesis was prepared by dissolving $Ni(NO_3)_2 \cdot 6H_2O$ (97% pure, Sigma-Aldrich, USA) in ethanol (99.5% pure, Sigma Aldrich, USA), followed by $CaCO_3$ addition (99% pure, Hayashi Pure Chemical Ind. Ltd., Japan). The suspension was stirred and the solvent was removed using a rotary evaporator (Hei-Vap Precision, Heidolph Instruments, Germany) at 50 °C under 100 mbar vacuum. The catalyst was dried overnight at 55 °C in an oven and calcined in air at 750 °C for 3 h to produce NiO supported on $CaCO_3$.

CNTs were synthesised according to the previously described procedure [9]. Briefly, the plastics (i.e. 1.5 g of pure LDPE or PP or 1.86 g of MP) were pyrolysed at 600 °C in a 50 mL min^{-1} N$_2$ flow for 30 min in a horizontal reactor. The produced non-condensable gases were converted in the vertical reactor into carbon nanomaterials over 0.5 g of the packed catalyst bed with particle sizes between 63 and 212 μm. In the preliminary experiments, it was observed that the entire temperature range between 500 and 800 °C was suitable for the growth of carbon nanomaterials using the prepared catalyst. Two synthesis temperatures were selected, namely 500 and 800 °C, in order to obtain pronounced differences in material morphology and properties. The concomitant mixed plastics without PET were used as feedstock to obtain CNTs at 500 °C and used as the sample of study (MP 500 °C). The obtained materials were boiled with 3 N HCl (EMD Millipore Corp., USA) for 30 min to dissolve calcium and nickel compounds, and filtered using 0.45 μm nylon filter (EMD Millipore Corp., USA). Subsequently, the suspension was washed repeatedly with deionised water and dried at 55 °C overnight. LDPE 500 °C, PP 500 °C and MP 500 °C were obtained at a carbon yield (percentage per catalyst mass) of 21, 32 and 3% respectively [9]. LDPE 800 °C, PP 800 °C and MP 800 °C were obtained at a carbon yield of 31, 22 and 22% respectively [9].

2.2. Materials for electrochemical experiments

N,N-dimethylformamide (DMF), potassium ferrocyanide trihydrate [$K_4Fe(CN)_6 \cdot 3H_2O$], potassium ferricyanide [$K_3Fe(CN)_6$], potassium chloride, potassium hydroxide, 20 wt% platinum on graphitised carbon (C/Pt) and concentrated sulphuric acid (95–98%) were purchased from Sigma Aldrich (Germany). Deionised water (18.2 MΩ cm) from a Millipore Milli-Q purification system was used in all the experiments. Alumina (0.05 μm) and micropolishing pad was obtained from (ALS, Japan).

2.3. Electrochemical apparatus

All voltammetric measurements were performed using an Interface 1000 Potentiostat (Gamry, USA) that was connected to a personal computer and controlled by Framework software (Gamry, USA). The electrochemical experiments were performed in an electrochemical cell (5 mL) at room temperature (25 °C) using a three-electrode configuration. A graphite plate was used as a counter electrode (4 × 4 × 80 mm) and an Ag/AgCl/KCl (saturated) electrode (ALS, Japan) was used as a reference electrode, while glassy carbon served as working electrode (diameter, 3 mm, obtained from CH Instruments, TX (USA)). The corresponding electrolyte solutions were saturated with air or nitrogen by bubbling air or nitrogen for 20 min. All electrochemical experiments have the current density normalised to the geometrical surface area of the electrode. The onset potential of oxygen reduction reaction is calculated from the deviation of the linear sweep voltammetry of the electrode material in the air-saturated 0.1 M KOH electrolyte in comparison to the nitrogen-saturated 0.1 M KOH.

Heterogeneous electron transfer experiments were carried out with 10 mM ferro/ferricyanide solution in 0.1 M KCl at a scan rate of 100 mV s^{-1}. The oxygen reduction reaction (ORR) was performed using linear sweep voltammetry (LSV) at a scan rate of 5 mV s^{-1} in air- and nitrogen-saturated 0.1 M KOH solution.

2.4. Dispersion of sample

A 5 mg mL^{-1} sample of CNT was suspended in DMF through sonication in a water bath using an ultrasonicator (37 kHz, Elma, S180H, Germany) for 30 min. Before the sample aliquot was prepared as an electrode material, the suspension was mixed again thoroughly through a sonication step for 5 min in the water bath. An aliquot of 1 μL of a 5 mg mL^{-1} sample was dropcasted on the glassy carbon electrode surface. The sample was then left to dry under an incandescent lamp for 10 min and used in the electrochemical experiment. Electrode surface was renewed using 0.05 μm alumina slurry and micropolishing pad.

2.5. Microscopic and spectroscopic characterisation of CNTs

Scanning electron microscope (SEM) images of carbon nanomaterials were taken using field emission scanning electron microscopy (FESEM, JEOL JSM-7600F) coupled with energy dispersive X-ray spectroscope (EDS, Oxford Xmax80 LN2 Free). Raman spectroscopy was carried out by casting the powder sample on a glass microscope slide before being sent for analysis by a Raman Spectrometer (XploRA PLUS, Horiba Scientific, Japan) coupled with a 532 nm laser source. X-ray photoelectron spectroscopy (XPS) was measured with Kratos Axis Supra spectrometer with a dual anode monochromatic Kα excitation source. Binding energies (B.E.) of the elements were calibrated against C 1 s core level at 284.5 eV. The nickel concentration was measured by using an inductively-coupled plasma-optical emission spectrometer (ICP-OES: Perkin Elmer Optima 8000). Namely, 10 mg of the CNTs sample was digested in a 9 mL of 60% fuming HNO$_3$ (Sigma-Aldrich) and 2 mL of stabilised 30% H$_2$O$_2$ (Merck) mixture under microwave irradiation at a temperature of 180 °C for 20 min. The solution was allowed to cool down before being filtered using a 0.45 μm PVDF syringe
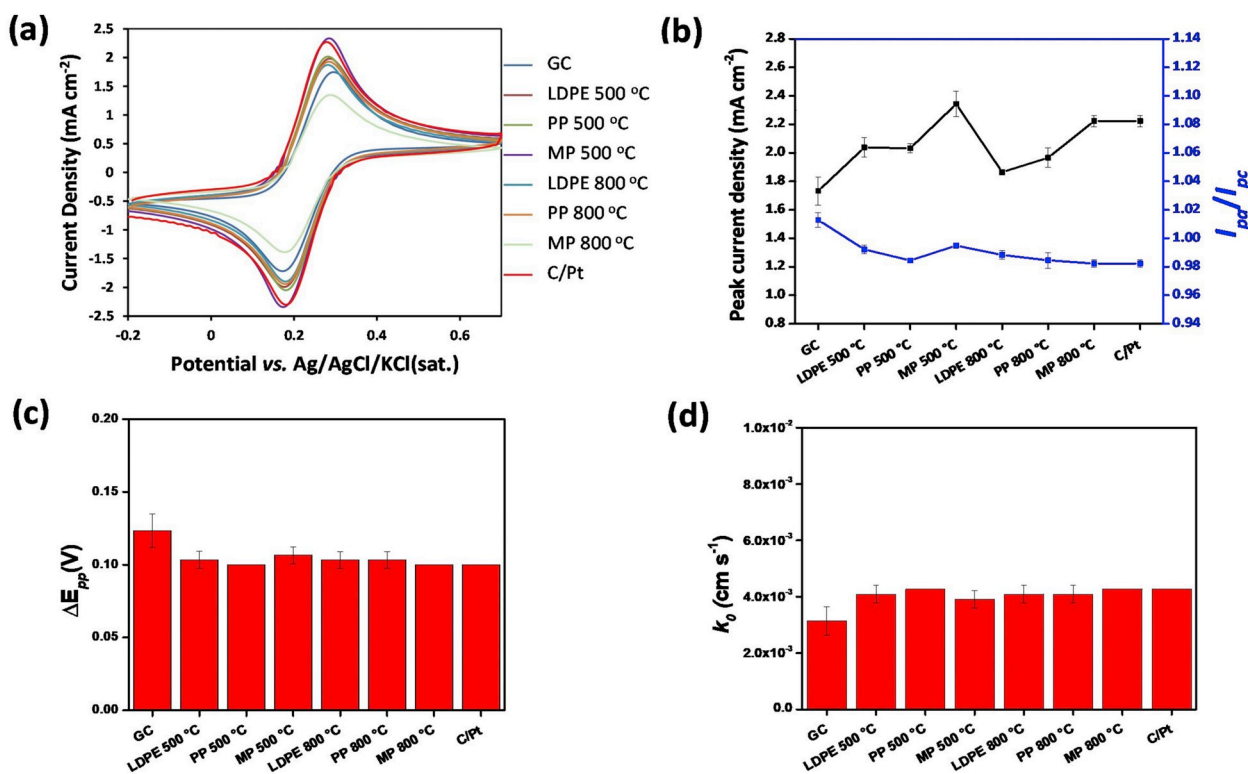
Fig. 1. (a) Cyclic voltammograms of the different modified glassy carbon (GC) electrode surfaces in 10 mM $Fe(CN)_6^{3/4-}$ in 0.1 M KCl at a scan rate of $100\,mV\,s^{-1}$; (b) Comparison of the anodic peak currents of the ferricyanide probes on different electrode surfaces and the ratio of the anodic and cathodic peak (I_{pa}/I_{pc}); (c) Peak to peak potential differences (ΔE_{pp}) in the ferro/ferricyanide probe on different electrode surfaces; and (d) Heterogeneous electron transfer rate of ferro/ferricyanide probe on different electrode surfaces.

filter. The mixture was diluted ten times with deionised water and sent for analysis in the ICP-OES.

3. Results and discussion

A redox probe of ferricyanide/ferrocyanide was used to test the electrochemical performance of the CNTs synthesised from different feedstocks [21]. In Fig. 1(a), two electrochemical peaks were observed in a reversible reaction with a cathodic peak at 0.15 V and anodic peak at 0.28 V on the GC electrode. The peaks were from the reversible anodic oxidation of ferricyanide to ferrocyanide and the opposite cathodic reduction of ferrocyanide to ferricyanide in a 1:1 ratio as illustrated in Fig. 1(b). The anodic peak currents were observed to be higher in the materials that were synthesised at 500 °C as compared to 800 °C. The peak to peak separation (ΔE_{pp}) was measured between the anodic and cathodic peaks in Fig. 1(c), where better performance with smaller ΔE_{pp} values was observed in the CNTs in comparison to the control materials, i.e. GC and C/Pt. In Fig. 1(d), the corresponding electron transfer rates were calculated from the ΔE_{pp} [22,23,31], illustrating the electron transfer rates between 3.9×10^{-3} and $4.3 \times 10^{-3}\,cm\,s^{-1}$. This was more exemplary than that of GC at $3.1 \times 10^{-3}\,cm\,s^{-1}$ and close to C/Pt at $4.0 \times 10^{-3}\,cm\,s^{-1}$. These obtained data showcase that the synthesised CNTs can serve as excellent electrode materials that exhibit superior performance over common electrode materials with high quantities of electrochemically active sites. Carbon nanotubes have two regions capable of participating in electrochemical reactions: (1) the basal plane, consisting of two-dimensional conjugated sp^2 carbon atoms; (2) the edge defects, consisting of carbon atoms with dangling bonds and various oxygen surface functionalities. It is postulated that a higher density of edge defect sites is responsible for the enhanced electrocatalytic performance on a redox probe [32–34]. The availability of such edge defect sites allowed for the heterogeneous electron transfer from the electrode into the electrolyte

[33]. High density of defects in the as-synthesised CNTs was examined in ORR for possible applications as electrodes in fuel cells.

The CNTs were tested for their performance for ORR. ORR is an important electrochemical reaction at the cathode of the fuel cell [20]. Two distinct trends in the results were observed in Fig. 2(a). The CNTs synthesised at 500 °C outperformed the CNTs prepared at 800 °C in ORR in air-saturated 0.1 M KOH. The electrocatalytic performance of CNTs for ORR can be classified with into two bands and are grouped according to temperatures: 500 and 800 °C. With regards to the sources of plastics influencing the performances of the CNTs, there were only marginal differences between LDPE, PP and MP at the respective temperatures of 500 and 800 °C. From Fig. 2(b), the electrode surfaces modified with CNTs synthesised at 800 °C have ORR onset potentials of between −0.18 V to −0.21 V. However, electrode surfaces modified with CNTs synthesised at 500 °C have the earliest ORR potentials of between −0.11 to −0.14 V. CNTs synthesised from MP at 500 °C have the lowest onset ORR potential of −0.11 V. This electrochemical performance significantly exceeded the performance of glassy carbon (GC) electrode at −0.19 V and was comparable to platinum on carbon (C/Pt) electrocatalyst at −0.10 V. Edge defect sites have been listed as active sites for ORR [35–37], allowing adsorption processes of diatomic oxygen and its eventual reduction [38]. Increasing amount of these edge defects in carbon nanotubes has been demonstrated to enhance the ORR of CNTs [29,39,40].

Fig. 3 depicts representative FESEM images of carbon nanomaterials produced from CNTs at 500 and 800 °C. This was corroborated by the detailed TEM examinations showing that filamentous hollow carbon nanostructures with various diameters and lengths were synthesised, illustrating the presence of multi-walled carbon nanotubes [9]. The CNTs synthesised at 500 and 800 °C had outer diameters centred at 10–20 and 40–50 nm, respectively (Fig. S1, Supplementary information). At 500 °C, the chemical vapour deposition of non-condensable gases from decomposition of LDPE and PP resulted mainly in CNTs.
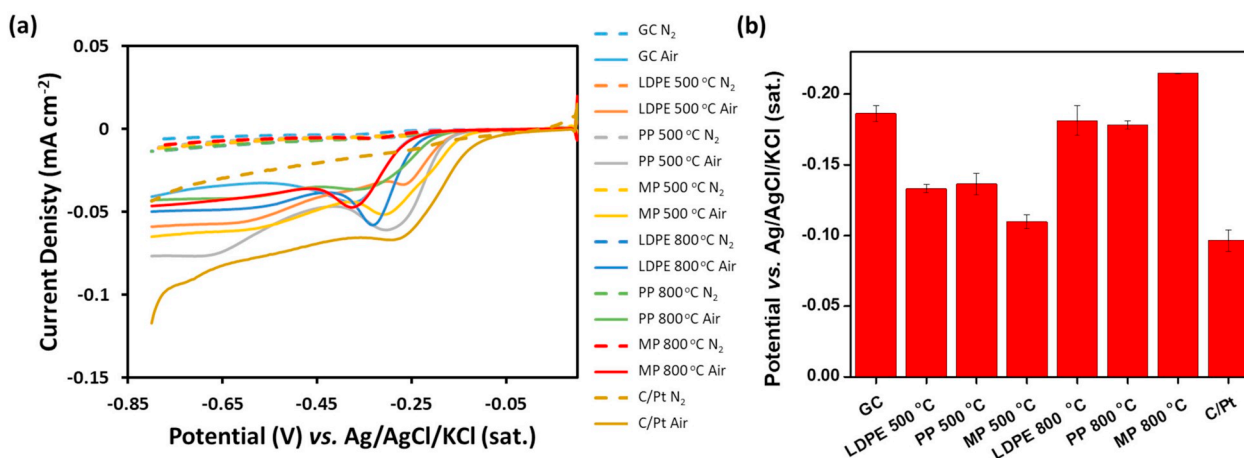
Fig. 2. (a) Linear sweep voltammograms (LSV) of oxygen reduction reaction (ORR) in electrolyte after saturation with nitrogen and air respectively. (b) Onset of ORR in air-saturated electrolyte, where the curve deviates from nitrogen-saturated electrolyte. Average of three scans were taken. Conditions: 0.1 M potassium hydroxide electrolyte, scan rate 5 mV s^{-1}.

Additionally, MP containing PET produced carbon nanocages [9]. The subsequent removal of PET from MP led to the increased selectivity towards CNTs.

Content from certain transition metal elements has been known to influence the electrochemical performance of carbon-based materials [41–45]. As illustrated in Fig. 4, it was found that CNTs synthesised at 500 °C had lower Ni contents (0.23–0.35 wt%), while the CNTs synthesised at 800 °C contained more Ni (4.2–6.3 wt%). MP 500 °C had the lowest metal content of 0.23 wt%, while MP 800 °C had the highest Ni content of 6.3 wt%. The higher Ni content in MP 800 °C was likely
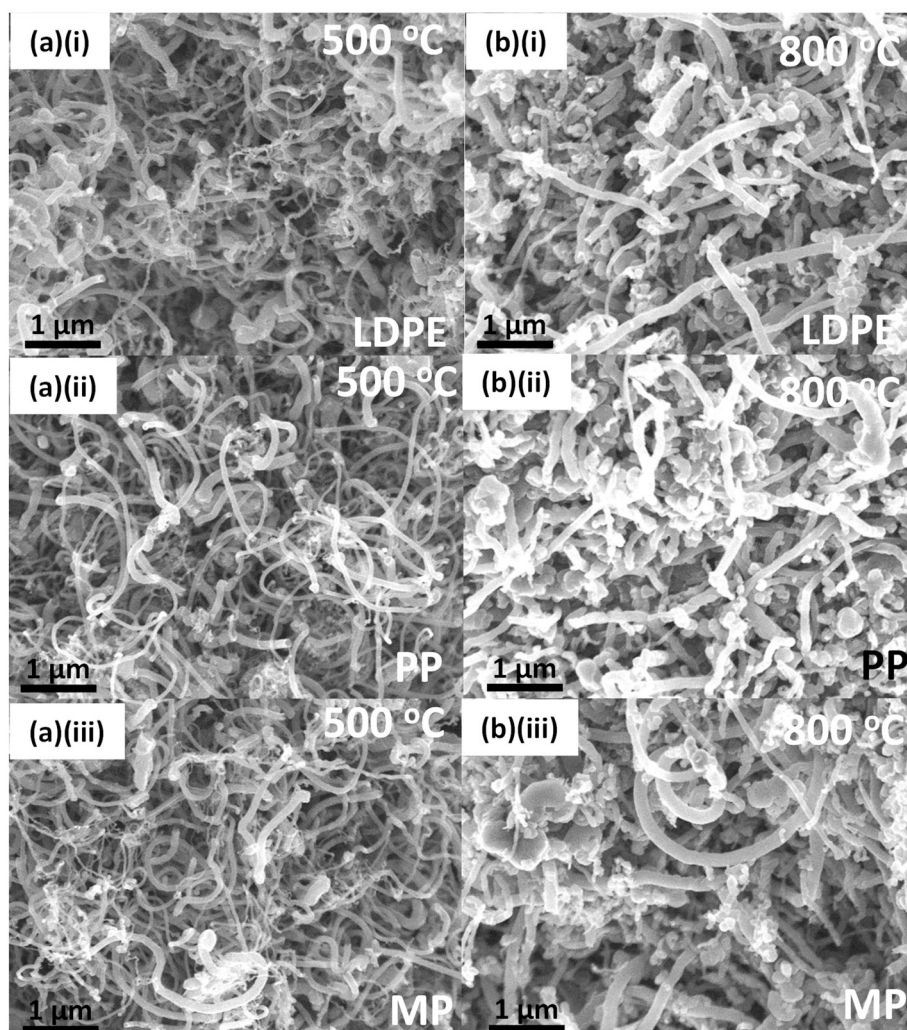

Fig. 3. FESEM images of CNTs fabricated at (a) 500 °C of (i) LDPE (ii) PP (ii) MP and at (b) 800 °C of (i) LDPE (ii) PP (ii) MP sources.
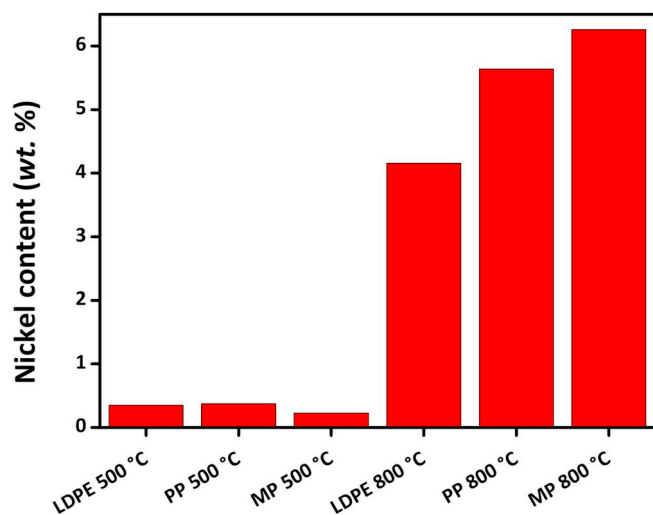
Fig. 4. Inductively-coupled plasma optical emission spectroscopy (ICP-OES) results of nickel content in carbon nanotubes after microwave digestion.

attributed to the larger thickness of carbon nanotubes, encapsulating the metal and preventing its removal during acid washing [41]. However, these differences in Ni content between CNTs synthesised at 500 and 800 °C did not influence the catalytic activities during ORR. Ni was likely embedded within the stems and sheaths of carbon sheets in the multi-walled CNTs [41], resulting in the negligible electrochemical efficacies as an electrocatalyst. Furthermore, the ORR is specific to certain metals, such as iron [46,47] and manganese [45] which are involved into the electrochemical reduction of intermediates or the diatomic oxygen. It has been demonstrated that Ni impurities in carbon materials has negligible effect on electrocatalytic activity during ORR [45]. Thus, the nickel content most likely does not govern the redox properties of synthesised CNTs during ORR.

Another possible reason influencing the catalytic activity of CNTs is the surface defects acting as active sites for the reactions. To get a better insight about surface defects that could determine the better performance of plastic-derived CNTs synthesised, the samples were characterized by Raman spectroscopy and XPS.

Raman spectroscopy is a good technique to characterize the density of edge defects present in carbonaceous materials [48]. The D band at 1340 cm^{-1} has been linked to structural disorder and sp^3-like edge defects and the G band at 1570 cm^{-1} has been linked to the sp^2-hybridised carbon vibrations [49,50]. The edge defects are typically located at the ends of the basal planes of CNTs [51]. An examination of the ratios of intensities between the D band G bands (I_D/I_G) calculated based on the peak height can be used to analyse the density of defects in the CNTs [49]. The Raman spectra for CNTs synthesised at 500 and 800 °C are displayed in Fig. 5. As illustrated in Fig. 5(a), the D band was more intense than the G band for the CNTs synthesised at 500 °C suggesting the higher density of defects compared to CNTs synthesised at 800 °C. In Table 1, the ratios of the intensities of D and G bands are provided. The I_D/I_G ratios of CNTs synthesised from LDPE, PP and MP at 500 °C were 1.49, 1.56 and 1.47, respectively, compared to 0.38, 0.38 and 0.39, respectively, at 800 °C. This demonstrated that at higher temperatures the CNTs were annealed and graphitised, resulting in a decrease in the density of defects. This was analogous to reports by Figarol et al. and Huang et al. where the decrease in density of structural defects was observed after heat treatment of CNTs at 2125 and 800 °C, respectively [52]. Yang et al. also demonstrated an annealing effect on CNTs when synthesis was carried out at higher temperatures [17]. This trend strongly correlated with the observed trend of ORR activity, where the CNTs synthesised at lower temperatures showcased lower overpotentials and better electrochemical performances. It was reported that high density of edge defects in

carbon nanomaterials corresponded to the higher electrocatalytic activity [21,32,53]. The edge defects in CNT-based materials are known to play an essential role during ORR [51,54–56]. On the other hand, oxygen functional groups, are known to retard electrochemical processes [57] and decrease the electrocatalytic activity of carbon-based materials during ORR due to stepwise two electron electrochemical reduction process to hydrogen peroxide before eventual reduction to water [58,59].

XPS is able to characterize the chemical oxidation states of the surface groups in carbonaceous nanomaterials. Survey XPS scan and high resolution XPS C 1 s analysis of the CNTs were conducted to provide the insight into the content of oxygen functional groups [50]. A survey XPS scan of the synthesised CNTs is a ready indicator of the distribution of surface oxygen functionalities in the CNTs synthesised at two different temperatures from different precursor sources [50,53]. Two different trends were noted in CNTs synthesised at two different temperatures. The amount of oxygen functionalities was lower in CNTs synthesised at 500 °C in comparison to the CNTs synthesised at 800 °C (Fig. 6). Table 2 demonstrates the numerical distribution of oxygen functionalities in the carbon nanomaterials. Carbon to oxygen (C/O) ratios were 20.9, 22.6 and 38.7 for CNTs synthesised from LDPE, PP and MP at 500 °C, respectively. These values were considerably higher than the C/O ratios of CNTs synthesised from LDPE, PP and MP at 800 °C (i.e. 18.6, 16.8 and 13.3, respectively). This could be explained by the introduction of oxygen functionalities into the carbon matrices at higher temperatures due to the presence of oxygen group impurities [60]. Huang et al. also demonstrated that with increasing annealing temperatures, there was an increase in the content of oxygen functionalities [61]. Thus, the catalytic synthesis of CNTs from non-condensable pyrolysis gases of plastics at 500 °C resulted in CNTs with lower oxidation degree. The lower oxidation degree was accompanied by the higher density of active edge defects in these CNTs as suggested by the Raman spectra [29]. MP 500 °C which has the highest C/O ratio in comparison to LDPE 500 °C and PP 500 °C has demonstrated the lowest ORR potential among the CNTs produced at 500 °C. This suggests that the combination of high defects and low oxidation degree is needed for a superior ORR performance. The superior electrocatalytic performance of CNTs produced at 500 °C was likely attributed to the combined effect of the both factors. Closer inspection of the high resolution C 1 s XPS spectra was needed to elucidate the type of oxygen functionalities present within the CNTs.

High resolution C 1 s XPS spectra can be used to analyse the surface oxygenated carbon functionalities on carbon nanotubes [62]. In the samples of CNTs synthesised from plastics, C=C, C−C, C−O and C=O groups with binding energies of 284.5, 285.4, 286.3 and 286.9 eV, respectively, were present. Carboxylic groups were absent in the samples. In case of the same feedstock, CNTs synthesised at 500 °C were less oxidised compared to 800 °C (Fig. 7). This is suggested by higher surface coverage with C=C groups (76–79% against 72–74% for the samples synthesised at 500 and 800 °C, respectively). The surface coverage of oxidised functional groups of C−C marginally increased from 16, 15, and 17% in LDPE, PP and MP at 500 °C, respectively, to 18, 18, and 20% at 800 °C, respectively. Introduction of oxygenated functionalities to carbon nanomaterials has been known to influence electrochemical properties [63–66]. Surface coverage of CNTs with oxygen functionalities was reported to decrease electrocatalytic activity of CNTs during ORR due to oxidative processes [63–65], and could explain the lower activity of CNTs synthesised at 800 °C. Surface oxygen functionalities of the C 1 s XPS spectra in CNTs also marginally increased from 5, 7, 7% to 9, 8, 8% in LDPE, PP and MP respectively when the synthesis temperature is increased from 500 to 800 °C. Previously from the survey XPS scan, it was shown that the density of these oxygen functionalities was higher in samples prepared at 800 °C because of the higher total oxygen content. Subsequently from this detailed C 1 s XPS spectrum, the proportion of the oxygen functionalities exhibited a marginal increase when synthesis temperatures were
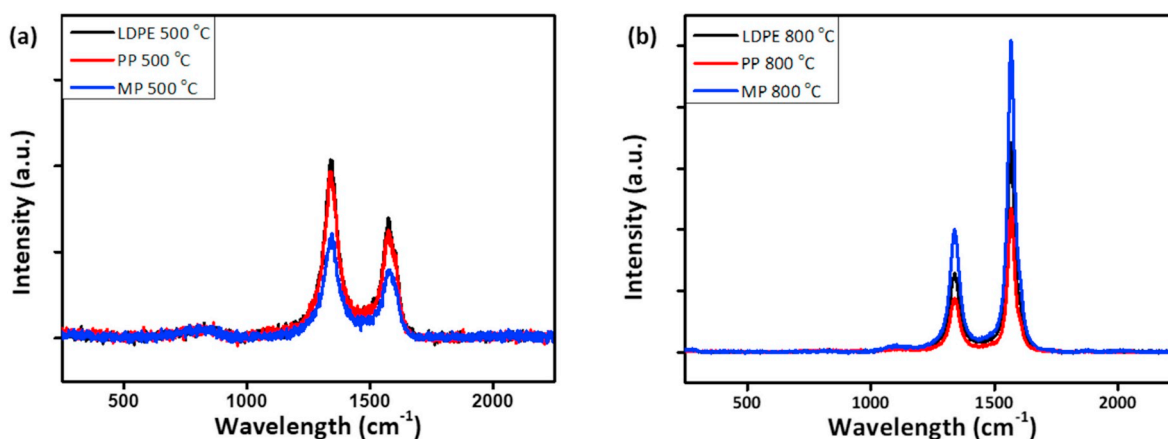
Fig. 5. Raman spectra of plastic-derived CNTs synthesised at (a) 500 °C (b) 800 °C.

Table 1
Ratios of intensity of D to G bands (I_D/I_G) in plastic-derived CNTs.

Samples	I_D/I_G	Samples	I_D/I_G
LDPE 500 °C	1.49	LDPE 800 °C	0.38
PP 500 °C	1.56	PP 800 °C	0.38
MP 500 °C	1.47	MP 800 °C	0.39

Table 2
Ratios of C/O intensities of CNTs synthesised at 500 and 800 °C in XPS survey scans.

Samples	C/O ratio	Samples	C/O ratio
LDPE 500 °C	20.9	LDPE 800 °C	18.6
PP 500 °C	22.6	PP 800 °C	16.8
MP 500 °C	38.7	MP 800 °C	13.3

increased from 500 °C to 800 °C. This showcased the effect of elevated synthesis temperatures on the increasing density of oxygen functionalities in CNTs. The increase in amount of C−C and oxygen functionalities from the XPS spectra with CNTs at 800 °C in comparison to those synthesised at 500 °C has decreased the amount of the defects that were capable of participating in ORR. It has been reported that higher temperatures have led to the termination of defects [64,65], with an increase in oxidised species [60], leading to a decrease in the electrochemical activity for ORR.

The edge sites responsible for heterogeneous electron transfer steps [54], with the corresponding oxidation of such sites leads to the decrease in electrochemical activity [57] and inhibits oxygen reduction [58,59]. Waki et al. reported that the presence of defect sites, particularly at the edges of carbon nanotubes, was the origin of

electrochemical activity during ORR [29,39,40]. Yang et al. suggested that extended exposure times at high temperatures led to the decrease in active edge defect sites due to graphitisation and resulted in the decreased performance during ORR [64]. Defects synthesised from temperature dependent processes [67,68], have been the origin of different electrochemical behaviours. Both XPS and Raman data were critical to forecast the electrochemical reactivity of CNTs synthesised from plastics.

4. Conclusion

The effects of synthesis temperature and feedstock on the performance of plastic-derived CNTs during electrocatalytic ORR was
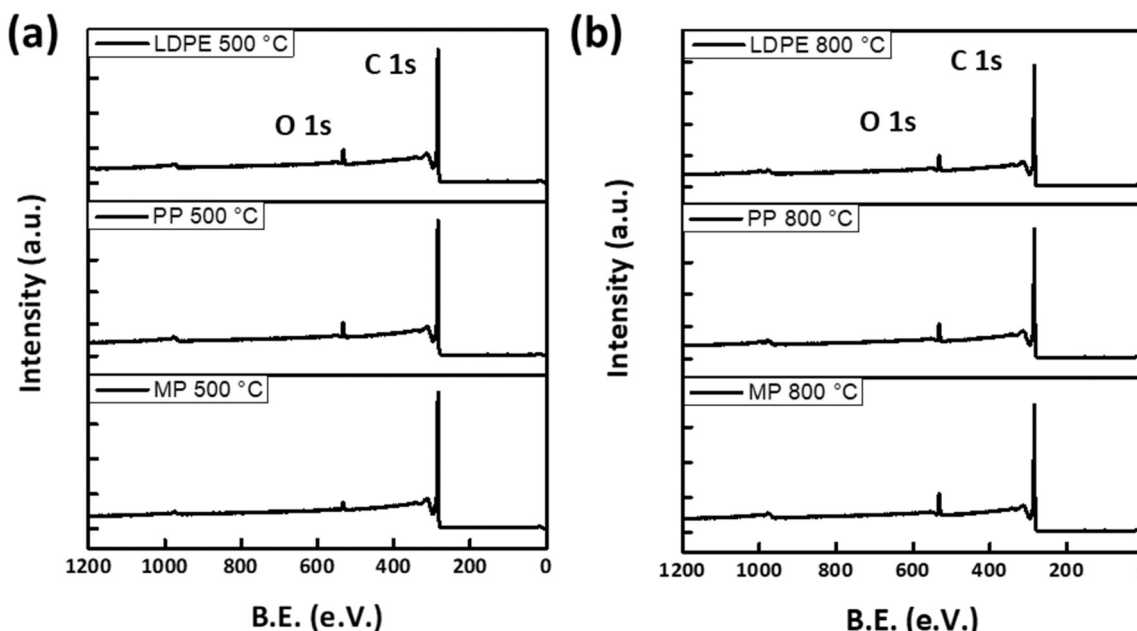

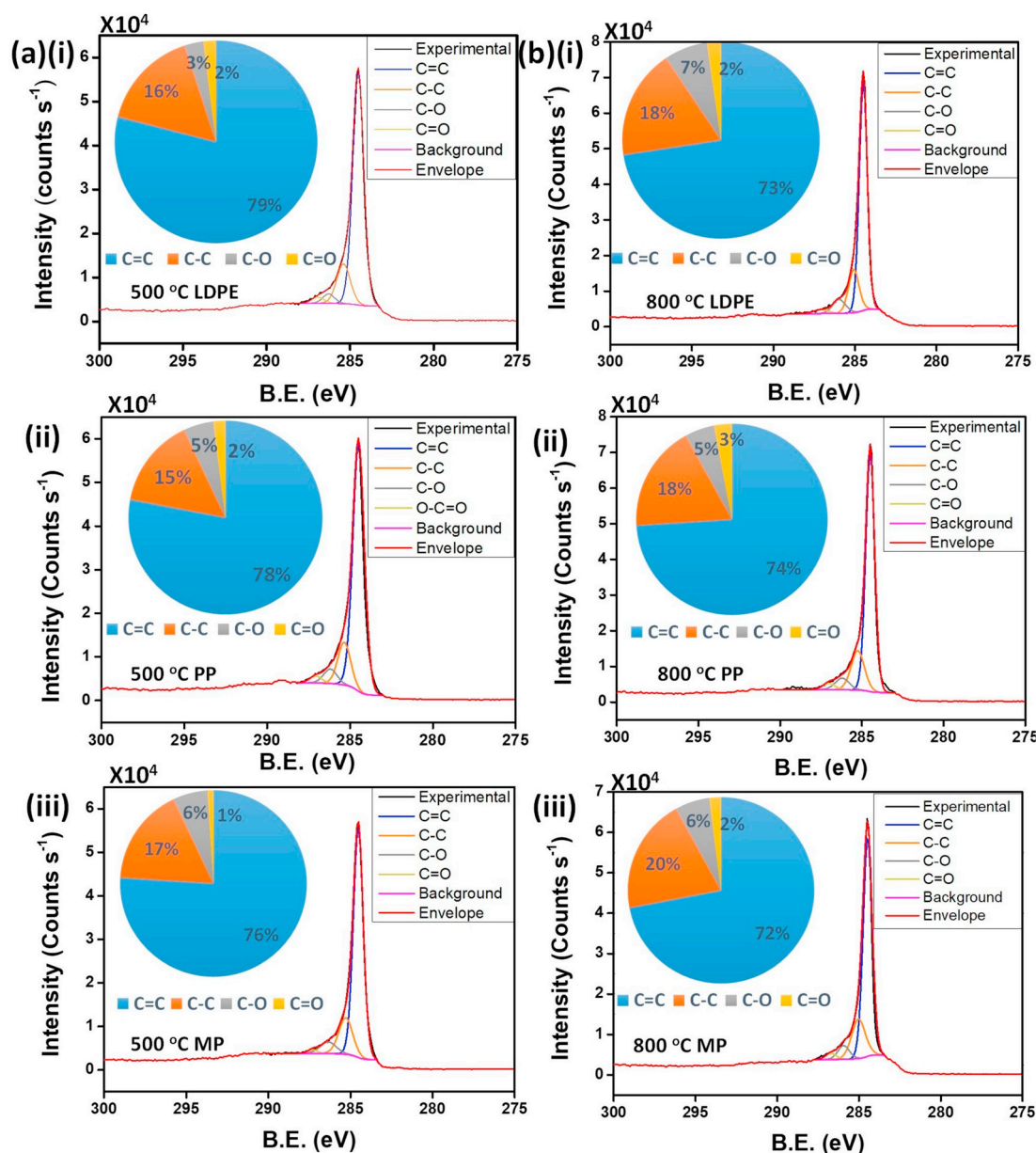**Fig. 6.** XPS survey scan spectra of CNTs fabricated at (a) 500 °C (b) 800 °C.

Fig. 7. High resolution XPS C1s scan spectra of CNTs fabricated at (a) 500 °C from (i) LDPE (ii) PP (iii) MP sources, at (b) 800 °C from (i) LDPE (ii) PP (iii) MP sources.

investigated. Synthesis temperature was the most important factor influencing the properties of CNTs and electrocatalytic activity. Namely, CNTs synthesised at 500 °C outperformed the CNTs synthesised at 800 °C. Raman spectroscopy has revealed that the CNTs at 500 °C contained a higher density of edge defects that can be utilized as active sites towards ORR, in comparison to CNTs synthesised at 800 °C. It can be reasoned that edge defective sites in plastic-derived CNTs have influenced the electrocatalytic performances during ORR, where an improved electrochemical performances have been observed at higher density of edge defective carbon sites. Larger amount of oxygen functionalities, as revealed by XPS, have decreased the ORR activity. On the other hand, influence of plastic feedstock (LDPE, PP, MP) on the electrocatalytic performance of ORR was found to be marginal. Predominantly, two bands of ORR potentials were observed and are grouped according to synthesis temperatures: CNTs synthesised at 800 °C have ORR onset potentials of between −0.18 to −0.21 V, while CNTs synthesised at 500 °C have the earlier and better ORR potentials of between −0.11 to −0.14 V. Waste plastic derived CNTs have been demonstrated to be a viable candidate as an electrode material,

especially for ORR. A clearer elucidation on the direct impact between synthesis procedures and electrocatalytic performance may serve to better plastic-derived CNT's capacities as an electrode material of choice. Wielding such capabilities, it is not unimaginable that plastics resources can recycled into electrode materials for energy-storage materials.

Acknowledgements

Appendix A. Supplementary data

Supplementary data to this article can be found online at https://doi.org/10.1016/j.elecom.2019.02.014.

References

[1] L.S. Diaz Silvarrey, A.N. Phan, Int. J. Hydrog. Energy 41 (2016) 16352–16364.
[2] W.R. Lea, J. Hazard. Mater. 47 (1996) 295–302.
[3] A. López, I. de Marco, B.M. Caballero, M.F. Laresgoiti, A. Adrados, A. Torres, Waste Manag. 31 (2011) 1973–1983.
[4] A. López, I. de Marco, B.M. Caballero, M.F. Laresgoiti, A. Adrados, Waste Manag. 30 (2010) 620–627.
[5] A. Adrados, I. de Marco, B.M. Caballero, A. López, M.F. Laresgoiti, A. Torres, Waste Manag. 32 (2012) 826–832.
[6] A. Veksha, A. Giannis, W.-D. Oh, G. Lisak, Chem. Eng. Sci. 189 (2018) 311–319.
[7] A.K. Panda, R.K. Singh, D.K. Mishra, Renew. Sust. Energ. Rev. 14 (2010) 233–248.
[8] X. Jia, C. Qin, T. Friedberger, Z. Guan, Z. Huang, Sci. Adv. 2 (2016) e1501591.
[9] A. Veksha, A. Giannis, V.W.C. Chang, J. Anal. Appl. Pyrolysis 124 (2017) 16–24.
[10] J. Gong, J. Liu, Z. Jiang, X. Wen, X. Chen, E. Mijowska, Y. Wang, T. Tang, Chem. Eng. J. 225 (2013) 798–808.
[11] D.S. Achilias, C. Roupakias, P. Megalokonomos, A.A. Lappas, E.V. Antonakou, J. Hazard. Mater. 149 (2007) 536–542.
[12] D. Yao, H. Yang, H. Chen, P.T. Williams, Appl. Catal. B 239 (2018) 565–577.
[13] A. Veksha, A. Giannis, W.-D. Oh, V.W.C. Chang, G. Lisak, Fuel Process. Technol. 170 (2018) 13–20.
[14] S.M. Al-Salem, P. Lettieri, J. Baeyens, Waste Manag. 29 (2009) 2625–2643.
[15] C. Wu, M.A. Nahil, N. Miskolczi, J. Huang, P.T. Williams, Process Saf. Environ. 103 (2016) 107–114.
[16] C. Wu, M.A. Nahil, N. Miskolczi, J. Huang, P.T. Williams, Environ. Sci. Technol. 48 (2014) 819–826.
[17] R.-X. Yang, K.-H. Chuang, M.-Y. Wey, Energy Fuel 32 (2018) 5462–5470.
[18] S. Ayyalusamy, S. Mishra, V. Suryanarayanan, Sci. Rep. 8 (2018) 13151.
[19] S. Sharma, G. Kalita, R. Hirano, S.M. Shinde, R. Papon, H. Ohtani, M. Tanemura, Carbon 72 (2014) 66–73.
[20] M.K. Debe, Nature 486 (2012) 43.
[21] R.L. McCreery, Chem. Rev. 108 (2008) 2646–2687.
[22] J.G.S. Moo, A. Ambrosi, A. Bonanni, M. Pumera, Chem. Asian J. 7 (2012) 759–770.
[23] J.G.S. Moo, M. Pumera, RSC Adv. 2 (2012) 1565–1568.
[24] M. Pumera, Chem. Euro. J. 15 (2009) 4970–4978.
[25] S. Iijima, Phys. B Condens. Matter 323 (2002) 1–5.
[26] R. Gusmão, E. Cunha, C. Paiva, D. Geraldo, F. Proença, F. Bento, ChemElectroChem 3 (2016) 2138–2145.
[27] R. Gusmão, Z. Sofer, M. Nováček, J. Luxa, S. Matějková, M. Pumera, Nanoscale 8 (2016) 6700–6711.
[28] Y. Li, W. Zhou, H. Wang, L. Xie, Y. Liang, F. Wei, J.-C. Idrobo, S.J. Pennycook, H. Dai, Nat. Nanotechnol. 7 (2012) 394.
[29] K. Waki, R.A. Wong, H.S. Oktaviano, T. Fujio, T. Nagai, K. Kimoto, K. Yamada, Energy Environ. Sci. 7 (2014) 1950–1958.
[30] J.C. Acomb, C. Wu, P.T. Williams, Appl. Catal. B 180 (2016) 497–510.
[31] R.S. Nicholson, Anal. Chem. 37 (1965) 1351–1355.
[32] D.A.C. Brownson, D.K. Kampouris, C.E. Banks, Chem. Soc. Rev. 41 (2012) 6944–6976.
[33] D.A.C. Brownson, S.A. Varey, F. Hussain, S.J. Haigh, C.E. Banks, Nanoscale 6 (2014) 1607–1621.
[34] C.E. Banks, R.G. Compton, Anal. Sci. 21 (2005) 1263–1268.
[35] S.M. Tan, C.K. Chua, D. Sedmidubský, Z. Sofer, M. Pumera, Phys. Chem. Chem. Phys. 18 (2016) 1699–1711.
[36] X. Chia, P. Lazar, Z. Sofer, J. Luxa, M. Pumera, J. Phys. Chem. C 120 (2016) 24098–24111.
[37] J. Xu, W. Huang, R.L. McCreery, J. Electroanal. Chem. 410 (1996) 235–242.
[38] M.S. Hossain, D. Tryk, E. Yeager, Electrochim. Acta 34 (1989) 1733–1737.
[39] T. Chen, J. Chen, K. Waki, Carbon 129 (2018) 119–127.
[40] J. Chen, K. Eguchi, K. Waki, ECS Trans. 80 (2017) 677–684.
[41] M. Pumera, Langmuir 23 (2007) 6453–6458.
[42] X. Chia, A. Ambrosi, P. Lazar, Z. Sofer, M. Pumera, J. Mater. Chem. A 4 (2016) 14241–14253.
[43] L. Wang, A. Ambrosi, M. Pumera, Angew. Chem. Int. Ed. 52 (2013) 13818–13821.
[44] M. Pumera, H. Iwai, J. Phys. Chem. C 113 (2009) 4401–4405.
[45] L. Wang, M. Pumera, Chem. Commun. 50 (2014) 12662–12664.
[46] M. Pumera, H. Iwai, Chem. Asian J. 4 (2009) 554–560.
[47] M. Pumera, Y. Miyahara, Nanoscale 1 (2009) 260–265.
[48] A. Eckmann, A. Felten, A. Mishchenko, L. Britnell, R. Krupke, K.S. Novoselov, C. Casiraghi, Nano Lett. 12 (2012) 3925–3930.
[49] C.K. Chua, M. Pumera, J. Mater. Chem. A 1 (2013) 1892–1898.
[50] S.M. Tan, A. Ambrosi, C.K. Chua, M. Pumera, J. Mater. Chem. A 2 (2014) 10668–10675.
[51] Z. Xu, X. Fan, H. Li, H. Fu, W.M. Lau, X. Zhao, Phys. Chem. Chem. Phys. 19 (2017) 21003–21011.
[52] A. Figarol, J. Pourchez, D. Boudard, V. Forest, S. Berhanu, J.-M. Tulliani, J.-P. Lecompte, M. Cottier, D. Bernache-Assollant, P. Grosseau, J. Nanopart. Res. 17 (2015) 194.
[53] A. Ambrosi, C.K. Chua, N.M. Latiff, A.H. Loo, C.H.A. Wong, A.Y.S. Eng, A. Bonanni, M. Pumera, Chem. Soc. Rev. 45 (2016) 2458–2493.
[54] L. Tao, Q. Wang, S. Dou, Z. Ma, J. Huo, S. Wang, L. Dai, Chem. Commun. 52 (2016) 2764–2767.
[55] T. Ishizaki, S. Chiba, Y. Kaneko, G. Panomsuwan, J. Mater. Chem. A 2 (2014) 10589–10598.
[56] I.-Y. Jeon, H.-J. Choi, S.-M. Jung, J.-M. Seo, M.-J. Kim, L. Dai, J.-B. Baek, J. Am. Chem. Soc. 135 (2013) 1386–1393.
[57] X. Ji, C.E. Banks, A. Crossley, R.G. Compton, ChemPhysChem 7 (2006) 1337–1344.
[58] J. Benson, Q. Xu, P. Wang, Y. Shen, L. Sun, T. Wang, M. Li, P. Papakonstantinou, ACS Appl. Mater. Interfaces 6 (2014) 19726–19736.
[59] D.-W. Wang, D. Su, Energy Environ. Sci. 7 (2014) 576–591.
[60] T.F. Zhang, K.-W. Kim, K.H. Kim, J. Electrochem. Soc. 163 (2016) E54–E61.
[61] C.-S. Huang, B.-R. Huang, Y.-H. Jang, C.-F. Hsieh, C.-C. Wu, M.-C. Chen, K.-L. Yang, MRS Proc. 828 (2004) A5.22.
[62] Z. Sofer, O. Jankovský, P. Šimek, K. Klímová, A. Macková, M. Pumera, ACS Nano 8 (2014) 7106–7114.
[63] Z. Liu, J. Xue, H. Yu, X. Yu, L. Feng, Energ. Technol. 6 (2018) 2394–2398.
[64] H.-J. Zhang, H. Li, X. Li, B. Zhao, J. Yang, Int. J. Hydrog. Energy 39 (2014) 16964–16975.
[65] H.-J. Zhang, H. Li, C. Deng, B. Zhao, J. Yang, ECS Electrochem. Lett. 4 (2015) H33–H37.
[66] R. Gusmão, V. López-Puente, I. Pastoriza-Santos, J. Pérez-Juste, M.F. Proença, F. Bento, D. Geraldo, M.C. Paiva, E. González-Romero, RSC Adv. 5 (2015) 5024–5031.
[67] N. Das, A. Dalai, J.S. Soltan Mohammadzadeh, J. Adjaye, Carbon 44 (2006) 2236–2245.
[68] C. Zhuo, J.O. Alves, J.A.S. Tenorio, Y.A. Levendis, Ind. Eng. Chem. Res. 51 (2012) 2922–2930.